Environmental Technology & Innovation 31 (2023) 103214

Contents lists available at ScienceDirect

Environmental Technology & Innovation

journal homepage: www.elsevier.com/locate/eti

Synthesis of Ni-Fe-CO_3 layered double hydroxide as Effective Adsorbent to remove Cr(VI) and ARS-dye from aqueous media

Ismail M. Ahmed [a,*], Ahmed I. Abd-Elhamid [b], Ashraf A. Aly [c], Stefan Bräse [d,e,*], AbdElAziz A. Nayl [a,*]

[a] Department of Chemistry, College of Science, Jouf University, Sakaka 72341, Aljouf, Saudi Arabia
[b] Composite and Nanostructured Materials Research Department, Advanced Technology and New Materials Research Institute (ATNMRI), City of Scientific Research and Technological Applications (SRTA-City), New Borg Al-Arab, Alexandria 21934, Egypt
[c] Chemistry Department, Faculty of Science, Organic Division, Minia University, El-Minia 61519, Egypt
[d] Institute of Organic Chemistry (IOC), Karlsruhe Institute of Technology (KIT), Fritz-Haber-Weg 6, 76133 Karlsruhe, Germany
[e] Institute of Biological and Chemical Systems – Functional Molecular Systems (IBCS-FMS), Hermann-von-Helmholtz-Platz 1, D-76344 Eggenstein-Leopoldshafen, Germany

ARTICLE INFO

Article history:
Received 28 March 2023
Received in revised form 4 May 2023
Accepted 15 May 2023
Available online 18 May 2023

Keywords:
Layered double hydroxides
Adsorption
Alizarine Red-S (ARS) and Cr(VI)

ABSTRACT

Ni^{2+}/Fe^{3+}LDH, (Ni-Fe-CO_3 LDH) with Ni/Fe molar ratio 3.0 was synthesized by co-precipitation for the remediation of chromium (VI), and Alizarine Red-S (ARS-dye) as anionic species. The investigated adsorbent was characterized by TGA, SEM, XRD, BET and FTIR. The effect of the hydrogen ion concentration of the medium, shaking time, ARS-dye and/or Cr(VI) concentration and adsorbents mass on the process was studied. The results of Ni-Fe-CO_3 LDH fitted well with the pseudo-second-order model. Langmuir isotherm is more favor than the Freundlich isotherm with maximum capacity (Q_{max}) of 69.9 and 6.1 mg/g for ARS-dye and Cr(VI), respectively.

1. Introduction

Annually, huge quantities of dye-contaminated wastewater are distributed into water bodies from many industrial activities (Khamis et al., 2020). This type of waste has harmful and poisonous effects on living organisms, human organs, and reduces the sunlight needed for aquatic plants to make photosynthesis (Rathinam et al., 2021). On the other hand, a large amount of toxic elements as chromium that results from various industrial applications and discharge into the surrounding environment (Khamis et al., 2020; Gautam et al., 2014). Cr(VI) is harmful as it causes irritation of the skin, eyes and respiratory tract and may lead to lung cancer (Zhang et al., 2019; Hadi et al., 2017). Synthetic dyes cause coloration of the effluent and the degradation of most of them are carcinogenic as anthraquinone — type dyes as Alizarine Red-S. Hence, in the field of wastewater treatment and to safeguard the environment, the removal of organic dyes and Cr(VI) is of utmost importance. Generally, several techniques were applied for the remediation of dyes and Cr(VI) as precipitation, coagulation, aerobic oxidation, solvent extraction, ion exchange, membranes and sorption (Peng et al., 2018; Jargalsaikhan et al., 2021; Genawi et al., 2020; Sheng et al., 2018; Yi et al., 2018, 2014; Chen et al., 2022; Hidalgo et al., 2020; Park et al., 2022). These methods have some limitations, though, in that even the degradable species of dye may be more hazardous. Sorption has an advantage over the abovementioned techniques as it is simple and of low operational cost. Recently more

* Corresponding authors.
E-mail addresses: imibrahim@ju.edu.sa (I.M. Ahmed), ahm_ch_ibr@yahoo.com (A.I. Abd-Elhamid), ashraf.shehata@mu.edu.eg (A.A. Aly), stefan.braese@kit.edu (S. Bräse), aanayel@ju.edu.sa (A.A. Nayl).

https://doi.org/10.1016/j.eti.2023.103214

attention was paid on layered double hydroxide (LDH) adsorbents, anionic clays that belong to hydrotalcite group due to ease of preparation in addition to their higher adsorption capacity towards organic dyes and heavy metals. The LDHs have a general formula $[M^{2+}_{1-x}\ M^{3+}_{x}\ (OH)_2.2A^{-m}{}_{x/n}\cdot\ mH_2O]$, where M is metal cation and A^{n-} is the interlayer anion (Ahmed, 2021). LDHs found many applications such as drug delivery, catalysts, gas sensors and adsorbents for the remediation of removal of toxic elements and organic dyes. The performance of LDH anion-exchange can be enhanced by changing the cation in the laminates, temperature, pressure, and solution pH during their preparation that affects the morphology of the obtained LDHs (Yao et al., 2017; Lu et al., 2016; Aguiar et al., 2013; Pahalagedara et al., 2014; Blaisi et al., 2018; Tan et al., 2016; Zhu et al., 2018; Dai et al., 2022; Amin et al., 2022; Jiang et al., 2022; Charafi et al., 2023; Mahieddine and Adnane-Amara, 2023; Li et al., 2016; El-Reesh et al., 2020; Chao et al., 2018; He et al., 2018; Intachai et al., 2022). In spite of their distinctive physicochemical features and the high ion exchange capacity, they have some drawbacks, such as mass loss during anion exchange and their relatively high-water solubility. In this respect, Ni-Fe LDHs have exceptional adsorption properties due to their large surface area and surface charge density. They have also been demonstrated to be effective at removing a number of pollutants from water, including heavy metals, dyes, and organic compounds. They are also considerably more economical than other LDHs. Ni-Fe LDH are a reliable option for water treatment applications since they have been found to have good stability over a variety of environmental conditions, such as pH, temperature, and salinity. In addition to their relatively low solubility product (p*K*sp = 60.81) (El-Reesh et al., 2020). In this study, Ni-Fe-CO_3 LDH, the factors influence the sorption processes as the effect of pH, initial Cr(VI) and ARS-dye concentrations, equilibration time, adsorbent mass and temperature were investigated for the remediation of Cr(VI) and ARS-dye as anionic species . A comparison study was looked into to gauge effectiveness of the prepared Ni-Fe-CO_3 LDHs to remove Cr(VI) and ARS-dye as anionic species with other recently published works.

2. Experimental

All chemicals were used without further purifications, distilled water extracted with a purification system was used Milli-Q direct 8 purifications (Millipore, France).

2.1. Synthesis of Ni-Fe-CO_3 LDH

250 mL of 1.5 M $NiCl_2{\cdot}6H_2O$ and 0.5 M $FeCl_3$ were added drop wise to 50 mL mixture of NaOH (1.0 M) and Na_2CO_3 (2.0 M) with vigorous stirring for 2.0 h and maintaining the pH of 11.0 ± 0.1. The slurry formed was aged at 80 °C for 5.0 days, centrifuged, washed with distilled water and finally, dried at 80 °C overnight before being used.

2.2. Instrumentation

XRD of LDH was characterized using a Shimadzu XRD-7000 diffractometer. The concentrations of Cr(VI) and/or ARS were investigated by Perkin Elmer UV–Visible Spectrophotometer . FT-IR spectra were performed using (FTIR)IR – Tracer 100, Shimadzu, Japan. The BET was characterized utilizing Quantachrome, NOVA 4200 e series, USA. The morphology of LDH was studied by Thermo Scientific Quattro ESEM, USA. The thermal decomposition behavior was examined by a Shimadzu, TGA 51.

2.3. Sorption of Cr(VI) and ARS-dye onto Ni-Fe-CO_3 LDH

0.025 g of the Ni-Fe-CO_3 LDH was equilibrated with 10.0 mL of and 10.0 mg/L for Cr(VI) or ARS-dye at pH 6.0, unless otherwise was stated. ARS-dye concentration was measured by UV–Vis spectrophotometer at λ_{max} 555.0 nm while Cr(VI) was estimated using 1,5-Diphenylcarbazide method at λ_{max} 545.0 nm (Marzenko, 1986). The removal percent was estimated as follow:

$$R\% = \left(\frac{C_o - C_e}{C_o}\right) \times 100 \tag{1}$$

Where $C_\circ$ and C_e are the initial and equilibrium concentration, respectively.

3. Results and discussion

3.1. Characterization of Ni-Fe-CO_3 LDH

3.1.1. TGA

TGA is used to evaluate the thermal behavior materials. The Ni-Fe-CO_3-LDH shows two decomposition steps refer to the surface moisture, interlayer water and hydroxyl groups (12.5%, 25–200 °C). The second (from 200 to 350 °C) is due to partially decarboxylation, mass loss of 15.6% (Cardinale et al., 2022), Fig. 1.

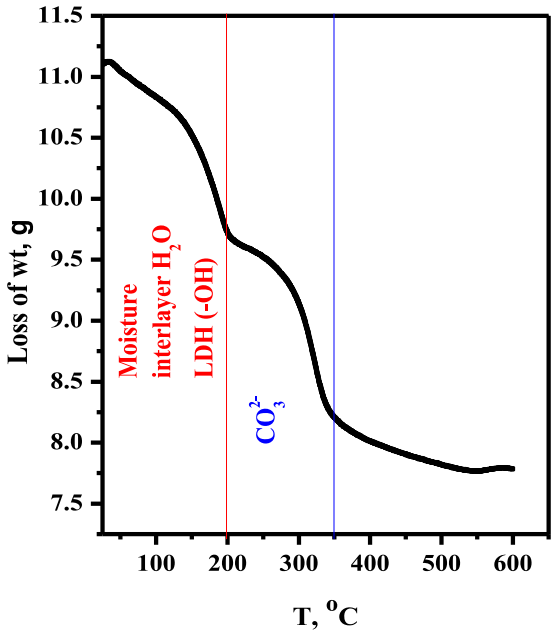

Fig. 1. The thermogravimetric analysis (TGA) of Ni-Fe-CO_3 LDHs.

3.1.2. SEM

The SEM instruments are utilized as an effective technique to detect the morphology of the surface of the Ni-Fe-CO_3 LDH. To understand the efficiency of the sorption technique, SEM images of the surfaces of Ni-Fe-CO_3 LDH was represented in Fig. 2. As shown in Fig. 2, 3D hierarchical micro/nanostructures were formed with various types of textural pores that clearly appeared with increasing the magnifications (Habib et al., 2020). The distinct morphologies are attributed to the presence of Ni^{+2} ions which reduces the surfaces energies difference between the polar- and nonpolar-planes (Habib et al., 2020; Kim et al., 2017). The fabricated Ni-Fe-CO_3-LDH materials illustrated aggregated flakes that create many cavities that can enhance the adsorption processes of anionic species (Qi et al., 2011).

3.1.3. FTIR

FT-IR spectra in Fig. 3, before and after sorption show very characteristic bands for the hydrotalcite-like phases. The pre-adsorption (a) band at 3439 cm^{-1} that refer to the stretching vibration of hydroxyl group, bending vibration of water appears at 1633 cm^{-1} while carbonate vibration appears at 1360 cm^{-1}. The three peaks at 400–700 cm^{-1} that refers to correspond to M–O (M: Ni^{2+}, Fe^{3+}) appeared in all LDHs samples. While the aromatic ring at ARS loaded LDH appears at 1016 cm^{-1}, the change in the FTIR spectra pre and post sorption confirms the complexation between LDH and both adsorbates (Flavio et al., 2008; Ahmet, 2009; Ayawei et al., 2015; Mališová et al., 2018; Xue et al., 2019).

3.1.4. XRD

XRD of Ni-Fe-CO_3 LDH, Fig. 4, shows different diffraction peaks at $2\theta \approx$ 11.68, 23.27, 34.99, 36.76, 45.87, 61.5, and 65.31°, These peaks can be due to the 003, 006, 009, 012, 015, 110, and 113 diffraction peaks, respectively. The peaks (003), (006) and (009) are assigned to the lamellar material. While the diffraction peaks around 60° and 61.5° which correspond to carbonate anion (Wiyantoko et al., 2015) and by applying in Sherrer equation, the corresponding crystallite (grain) size was found to be 0.47 nm. Indeed, most of these peaks have straightly and symmetrically characteristics, completely proving that considerable purity of Ni-Fe-CO_3-LDH.

3.1.5. BET measurement

The surface area information can be deduced from the shape of adsorption isotherm. The adsorption isotherm of Ni-Fe-CO_3-LDH is mainly mesoporous in nature according IUPAC classification and classified as Type III (Sing, 1985). The measured BET surface area of Ni-Fe-CO_3-LDH is 110.70 m^2/g and the pore volume and pore size were 0.12 cc/g and 15.45 Å, respectively, Fig. 5.

3.2. Sorption investigations

3.2.1. Effect of pH

pH of the solution affects the nature of the adsorbent and adsorbate. The influence of medium pH was examined in the range 3.0–9.5 on the sorption behavior of Cr(VI) and ARS-dye using Ni-Fe-CO_3 LDH as adsorbent, Fig. 6. It is obvious that

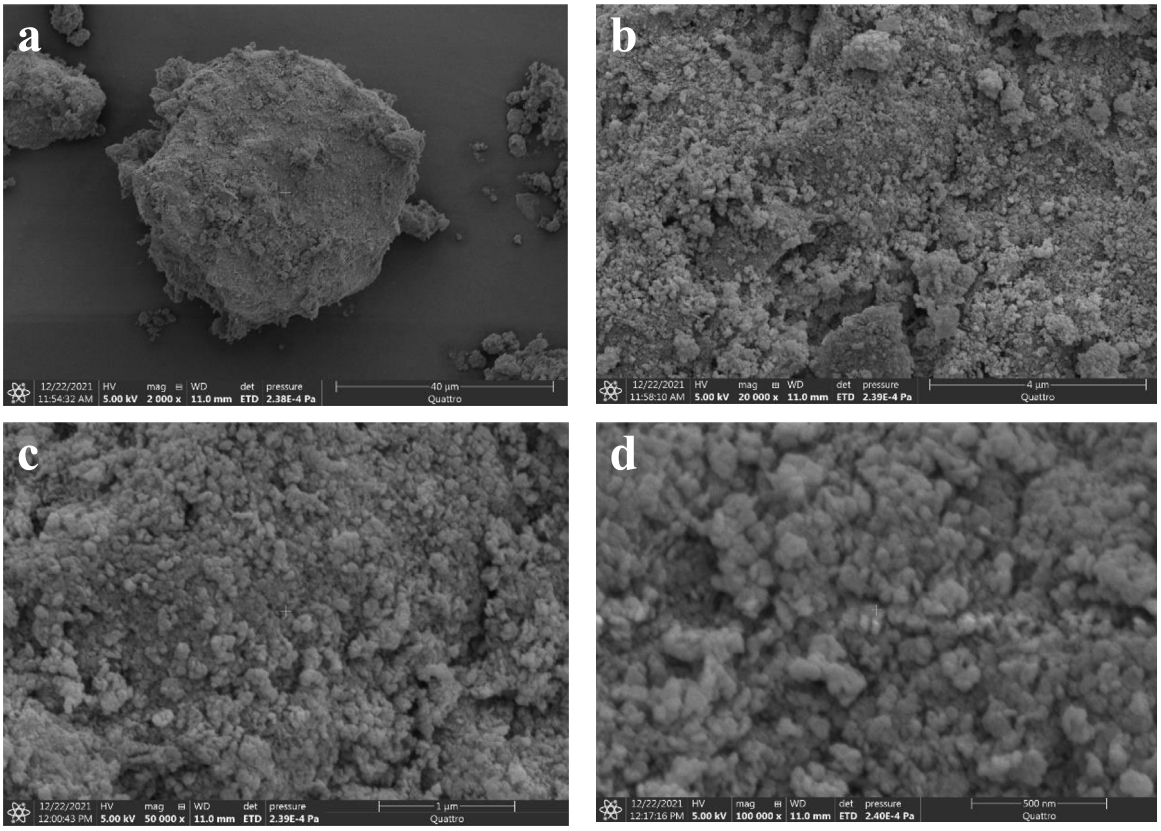

Fig. 2. SEM of Ni-Fe-CO_3 LDH with magnifications of (a) 2000x, (b) 20000x, (c) 50000x and (d) 100000x.

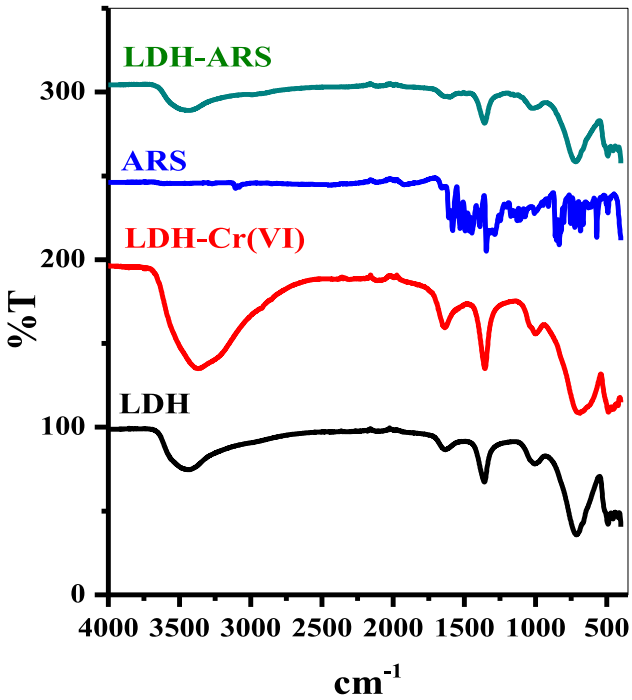

Fig. 3. FTIR of Ni-Fe-CO_3 LDH, Ni-Fe-CO_3 LDH-ARS, ARS and Ni-Fe-CO_3 LDH-Cr(VI).

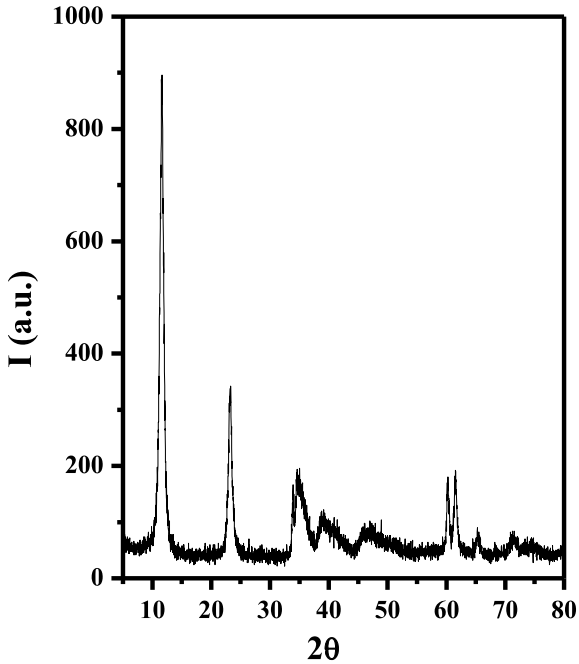

Fig. 4. XRD of Ni-Fe-CO_3 LDH.

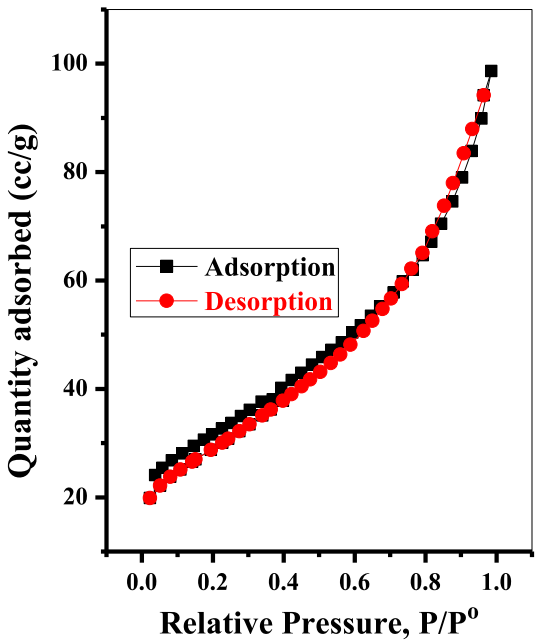

Fig. 5. Nitrogen adsorption/desorption isotherm of Ni-Fe-CO_3 LDH.

the sorption percent of both adsorbents remains constant in range (3.0–8.0) after this pH value the adsorption percent decrease for both adsorbates. In acidic medium the protonated binding sites of the adsorbent interact with -SO_3^- in the dye through electrostatic attraction and the anionic $HCrO_4^-$, $Cr_2O_7^{2-}$ and $HCr_2O_7^-$ species (Zolgharnein and Rastgordani, 2018; Khan et al., 2017) that favor the interaction with the protonated site. As the pH increases, the surface gains negative charge on the surface of LDH with anionic species (Zhang et al., 2013). The speciation of chromium(VI) can vary depending on the pH, ionic strength, and the presence of other ions or ligands in solution. In this respect, at pH 5.0, Cr(VI) exists primarily in the form of the hydrogen chromate ion $HCrO_4^- \gtrsim$ 90% in addition to the minor other oxo species dichroamte $Cr_2O_7^{2-}$and

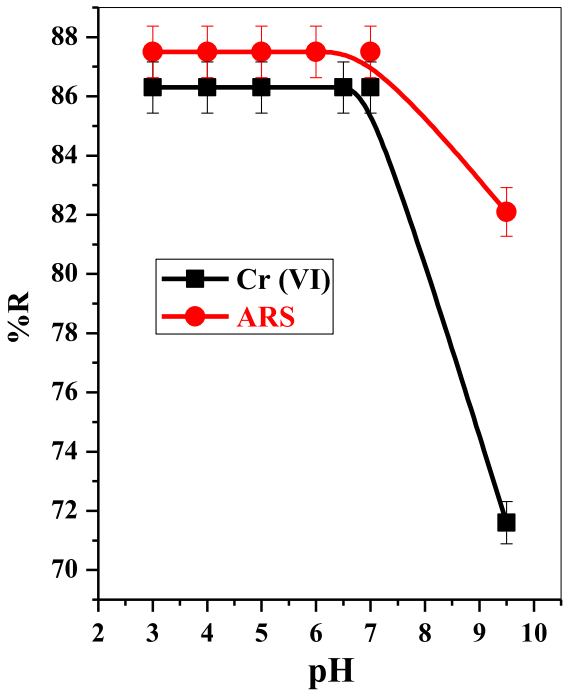

Fig. 6. Effect of pH on the adsorption of Cr(VI) and ARS-dye onto Ni-Fe-CO_3–LDH.

chromate ion CrO_4^- while at pH 1.0 chromic acid is the predominate species (Ahmed, I.M. and Hamed, M.M. and Metwally, S.S, 2020; Volf and Balan, 2013; Ajouyed et al., 2010; Tran, H.N. and Nguyen, D.T. and Le, G.T. and Tomul, F. and Lima, E.C. and Woo, S.H. and Sarmahg, A.K. and Nguyena, H.Q. and Nguyenh, P.T. and Nguyeni, D.D. and Vigneswaran, T.V. and Vo, D.N. and Chao, H.P., 2019) . It is worth to mention that the speciation of chromium(VI) is crucial in creating effective treatment strategies to remove chromium(VI) from wastewater or contaminated groundwater. The interaction between Cr(VI) and LDHs occurs through various mechanisms, including adsorption, surface complexation and ion exchange. In adsorption, the Cr(VI) ions are physically adsorbed onto the surface of the LDH through weak van der Waals forces or hydrogen bonding. In surface complexation, the Cr(VI) ions form chemical bonds with the surface functional groups on the LDH particles, such as hydroxyl or carboxyl groups. In ion exchange, the positively charged LDH surface attracts and holds onto the negatively charged Cr(VI) ions, similar to the ion exchange process with ion exchange resins. The ion exchange mechanism representing the possible interaction between the hydrogen chromate anion and the LDHs is given in Eq. (2) while Fig. 7 gives all possible interactions between LDH and CR dye.

$$Ni_6Fe_2\,(OH)_2\,CO_3.4H_2O + 2HCrO_4^- = Ni_6Fe_2\,(OH)_2\,(HCrO_4)_2.xH_2O + CO_3^{2-} \tag{2}$$

3.2.2. Effect of adsorbent dose

Ni-Fe-CO_3 LDH dose was discussed in the range 5.0–25.0 mg on the sorption percent of Cr(VI) and ARS-dye is plotted in Fig. 8. We noted that, the removal percent increase with the adsorbent dose due to increasing the available sites on LDHs surface.

3.2.3. Effect of contact time

The removal percentage of the two adsorbates onto Ni-Fe-CO_3 LDH was examined in the range (5.0–120 min), as presented in Fig. 9. The removal efficiency of both Cr(VI) and ARS-dye was increased rapidly up to 30 and 25 min. respectively. With increasing contact time, the removal percentage remained constant due to blocking the active sites with the progress of adsorption process (Goharshadi and Moghaddam, 2015).

Two kinetic models were studied to explain the adsorption behaviors. The pseudo first-order kinetics model that presented in Eq. (3)

$$\log(q_e - q_t) = \log q_e - (\frac{k_1}{2.303})t \tag{3}$$

The pseudo second order mechanism according to Eq. (4)

$$\left(\frac{t}{q_t}\right) = \left(\frac{1}{k_2 q_e^2}\right) + \left(\frac{1}{q_e}\right) t \tag{4}$$

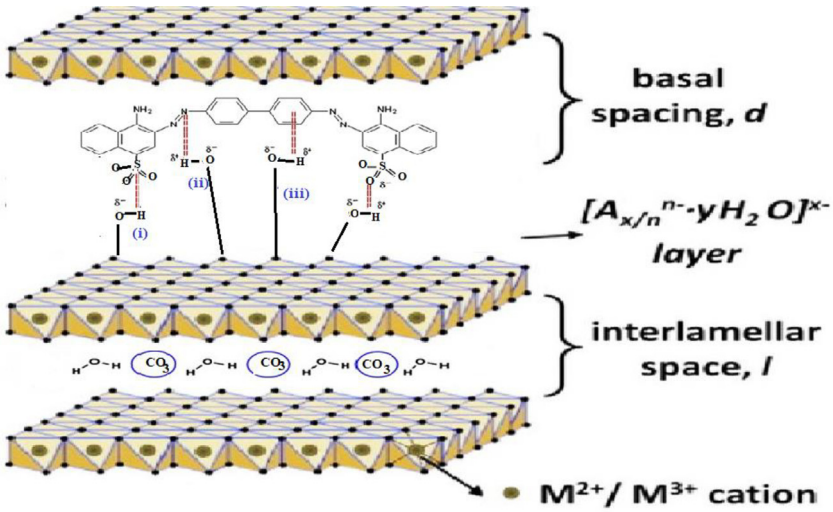

Fig. 7. CR dye-LDH interaction: (i) ionic interaction, (ii) hydrogen bonding between LDH and electronegative residues in the CR, and (iii) H-bonding between LDH and aromatic residue in CR molecule.

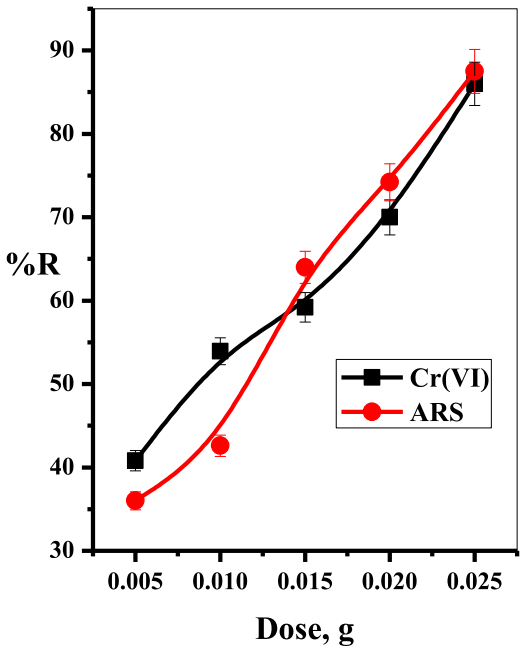

Fig. 8. Effect of adsorbent dose on the adsorption of Cr(VI) and ARS-dye onto Ni-Fe-CO_3–LDH.

where k_1 and k_2 are the rate constants of the pseudo first order and pseudo-second order, respectively, that were estimated from Fig. 10 and summarized in Table 1. The sorption of ARS-dye and Cr(VI) obey the pseudo-second-order model considering that the q_e(cal) values are near to q_e(exp).

3.2.4. Effect of initial concentration

The effect of initial Cr(VI) and ARS-dye concentration on the adsorption was investigated in the range (10–100 mg/L) and (100–400 mg/L), respectively. Fig. 11. It is obviously noted that the sorption of both adsorbate increases with increasing the initial concentration this is due to presence of available adsorbate molecules adsorption process.

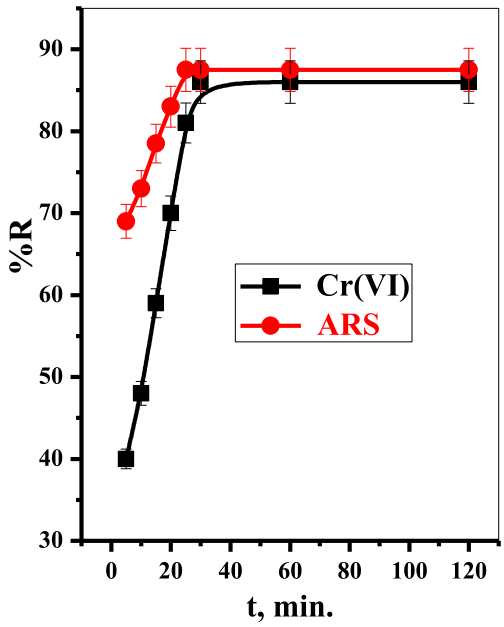

Fig. 9. Effect of contact time on the adsorption of Cr(VI) and ARS-dye onto Ni-Fe-CO_3–LDH.

Table 1
Calculated parameters of the pseudo-first-order and pseudo-second-order kinetic models.

Pollutant	T, °K	q_{eexp} (mg/g)	First-order kinetic parameter			Second-order kinetic parameter		
			K_1(min^{-1})	q_{ecal} (mg/g)	R^2	K_2(g mg^{-1}min^{-1})	q_{ecal}(mg/g)	R^2
Cr(VI)	298	3.44	0.106	4.06	0.853	0.019	4.50	0.913
	308	3.71	0.107	4.26	0.818	0.023	4.47	0.918
	318	3.92	0.149	3.75	0.917	0.030	4.45	0.967
	328	3.96	0.102	3.12	0.972	0.038	4.41	0.988
ARS-dye	298	35.0	0.094	13.30	0.956	6.96×10^{-4}	35.74	0.996
	308	35.6	0.094	11.67	0.960	7.24×10^{-4}	35.97	0.998
	318	38.1	0.101	13.00	0.982	5.97×10^{-4}	38.79	0.999
	328	39.4	0.089	12.13	0.955	5.86×10^{-4}	39.68	0.998

The experimental data were analyzed by Langmuir and Freundlich models. In linear form of Langmuir isotherm is represented according to Eq. (5):

$$\left(\frac{C_e}{q_e}\right) = \left(\frac{1}{Q_{max}\mathrm{b}}\right) + \left(\frac{1}{Q_{max}}\right) C_e \tag{5}$$

Where, Q_{max} is the monolayer capacity and b is the binding energy between the adsorbent and the adsorbate. The results are illustrated in Fig. 11 and Table 2. Separation factor or equilibrium parameter R_L can be estimated from Eq. (6).

$$R_L = \frac{1}{1 + bc_o} \tag{6}$$

The adsorption of both systems was found to be favorable, linear, and the adsorption is irreversible (Mane and Vijay Babu, 2013). Q_{max} was found to be 6.1 and 69.93 for Cr(VI) and ARS-dye, respectively while $0 < R_L < 1$ that means that the sorption processes are favorable.

The linear equation of Freundlich model is given as:

$$\log q_e = \log K_f + (1/n) \log C_e \tag{7}$$

Where, K_f and n are the adsorption performance and intensity, respectively and can be computed from plotting log q_e against log C_e, Fig. 11; and Table 2. Indeed, Langmuir isotherm is more favors than the Freundlich isotherm for both systems.

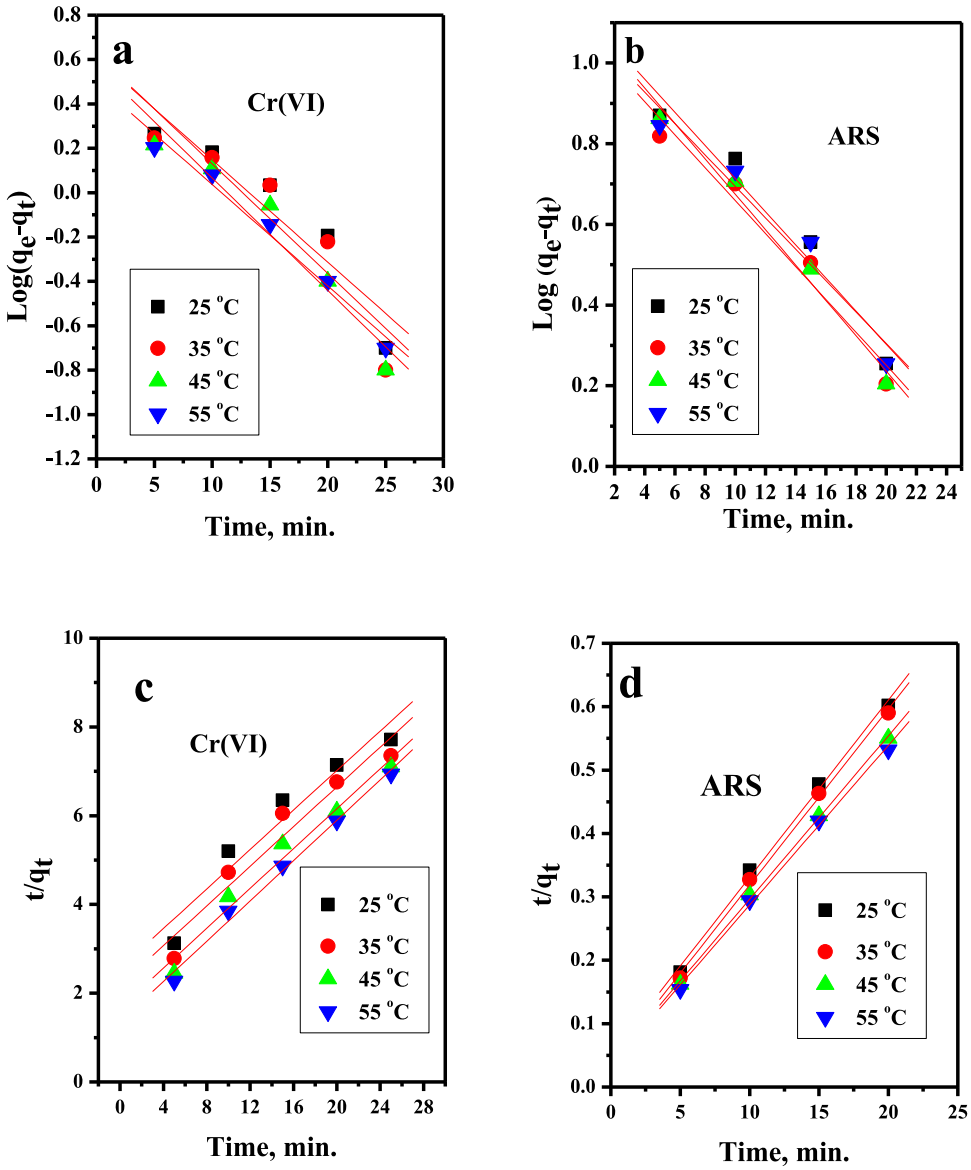

Fig. 10. Pseudo-first-order and pseudo-second-order models for the adsorption of Cr(VI) and ARS-dye onto Ni-Fe-CO_3–LDH.

Table 2
Calculated equilibrium constants for adsorption of Cr(VI) and ARS-dye onto Ni-Fe-CO_3 LDH.

Pollutant	Langmuir isotherm model				Freundlich isotherm model		
	q_e(mg/g)	b (l/mg)	R_L	R^2	1/ n	K_f (mg/g)	R^2
Cr(VI)	6.10	0.36	0.217	0.996	0.206	20.04	0.950
ARS-dye	69.93	0.036	0.217	0. 974	0.178	3.45	0.964

3.2.5. *Effect of temperature*

The influence of temperature on the removal of Cr(VI) and ARS-dye onto Ni-Fe-CO_3-LDH adsorbent was investigated in the range 298-328 °K, Fig. 12. The sorption increases with temperature, and this may refer to increasing in the rate of diffusion into the internal pores of the adsorbent particle from the external boundary layer (Weber, 1972; Jain and Sikarwar, 2008).

The thermodynamic parameters can be estimated from the following equations (Eqs. (8) and (9)):

$$\ln K_D = \frac{\Delta S^o}{R} - \frac{\Delta H^o}{RT} \tag{8}$$

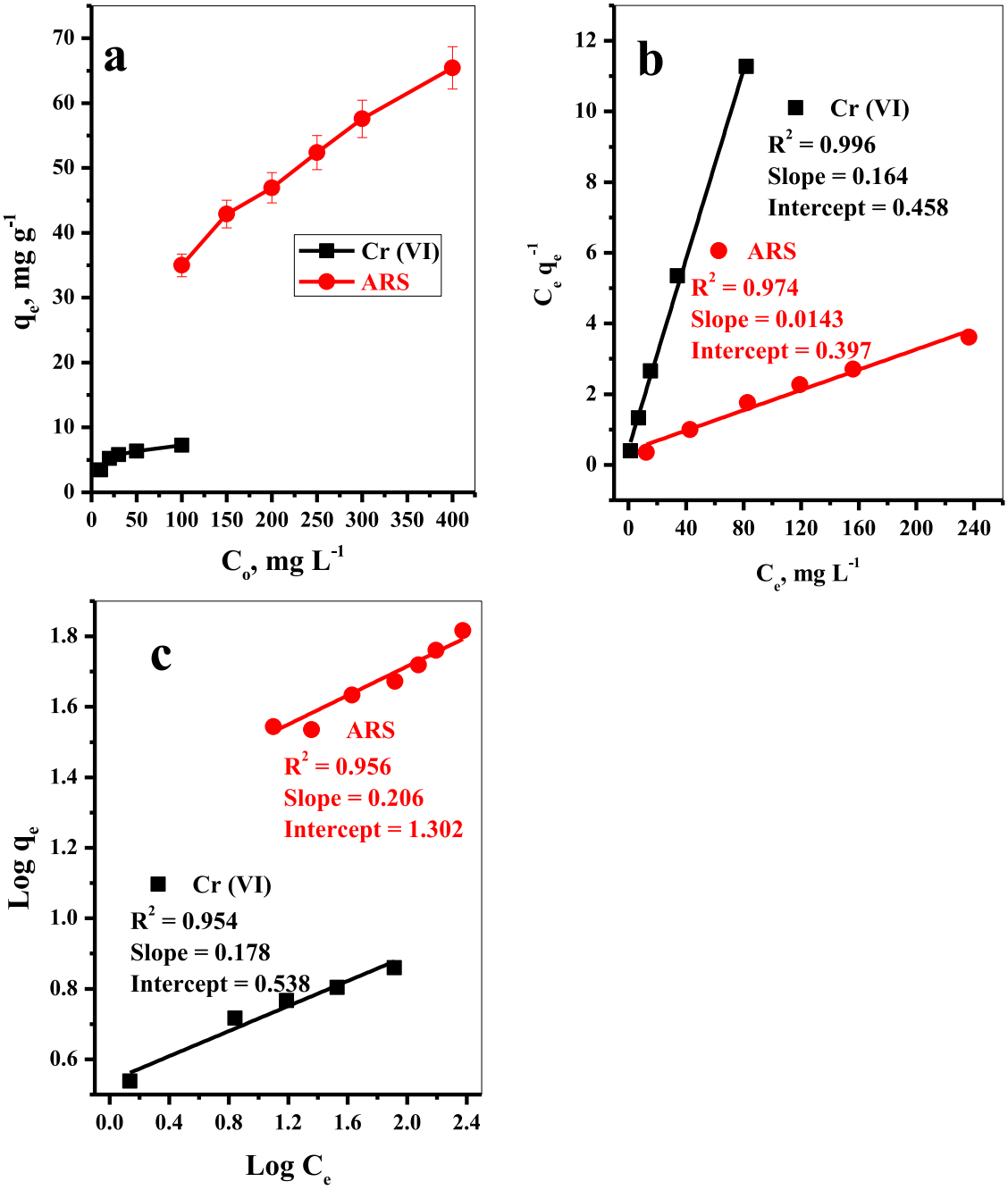

Fig. 11. (a) Effect of initial concentration of Cr(VI) and ARS-dye onto Ni-Fe-CO_3–LDH, (b) Freundlich's adsorption isotherm, and (c) Langmuir's adsorption isotherm.

$$\Delta G^o = \Delta H^o - T\Delta S^o \tag{9}$$

The positive value of ΔH° (30.25 and 17.78 kJ/mol) indicates the endothermic character of the process. The value of ΔH° indicates physisorption where van der Waals interaction, hydrophobic interaction and electrostatic attraction. The positive ΔS° value suggests an increase in the randomness of the system and the negative value of ΔG° indicates that the adsorption is spontaneous and favored at higher temperature and indicating the process is physical process as the ΔG° values ranging from −20 to 0 KJ/mol (Li et al., 2010) also, ΔH°, ΔS° and ΔG° were also given in Table 3.

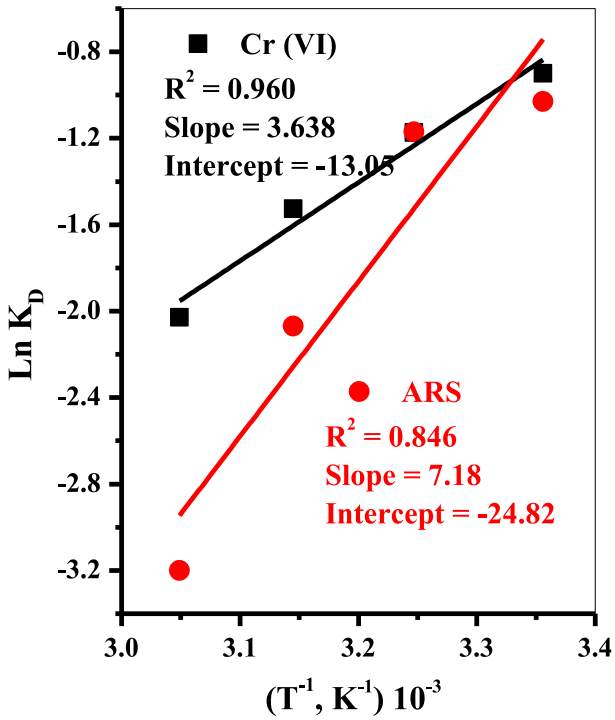

Fig. 12. Effect of temperature on sorption of Cr(VI) and ARS dye onto Ni-Fe-CO_3–LDH.

Table 3
Thermodynamic parameters for sorption of Cr(VI) and ARS dye onto Ni-Fe-CO_3–LDH.

	T, °K	ΔH^o (KJ/mol)	ΔS^o (J/mol)	ΔG^o (KJ/mol)
Cr(VI)	298	30.25	108.46	−2.08
	308			−3.16
	318			−4.27
	328			−5.33
ARS	298	17.78	206.39	−43.72
	308			−45.79
	318			−47.85
	328			−49.92

3.3. Comparison study

Table 4 represented a comparison between the efficiency of **Ni-Fe-CO_3–LDH** as adsorbents with other adsorbent materials used in the sorption processes of Cr(VI) and ARS-dye (Bhattarai et al., 2022; Ahmed et al., 2020; Alshammari et al., 2021; Nayl et al., 2022; Bagbi et al., 2017; Kumar et al., 2018; Abukhadra et al., 2019; Bhomick et al., 2020; Badran and Khalaf, 2020; Fayazi et al., 2015; Gholivand et al., 2015; Bharath et al., 2022; Machado et al., 2016). The results obtained illustrate that **Ni-Fe-CO_3–LDH** gives a considerable capacity and efficiency for the Cr(VI) and ARS-dye adsorption.

3.4. Desorption study

Regeneration of spent adsorbent is of great economic importance. In this respect, sodium hydroxide solution of concentration (0.01–0.1 M) showed recovery of Cr(VI) and ARS dye Alizarine ≈ 95% .

4. Conclusion

In this work, Ni-Fe-CO_3 LDHs was investigated for the sorption of Cr(VI) and ARS dye as anionic species in batch systems. Adsorption process fitted pseudo-second order and obey the Langmuir model with monolayer sorption capacity Q_{max} of 6.1 and 69.9 mg/g for Cr(VI) and ARS-dye, respectively. The thermodynamic parameters indicated that the sorption process is endothermic, spontaneous with increasing the randomness of the system. Reuse of the adsorbent was attained using caustic soda solution of concentration (0.01–0.1 M) and the desorption percentages reached ≈ 95%.

Table 4
Q_{max} of Ni-Fe-CO_3–LDH compared with recently reported adsorbent materials to remove Cr(VI) and ARS-dye.

Pollutant	Adsorbent	Q_{max}, mg/g	pH	Ref.
Cr(VI)	Arundo donax Stem biosorbent	76.9	2.0	57
	Fe_3O_4-coated perlite	8.8	2.0	58
	Fe_2O_3/HMS composite	10.8	2.0	59
	Magnetite Talc (Fe_3O_4@Talc) Nanocomposite	13.5	2.0	60
	L-Cysteine magnetite	34.5	2.0	61
	Zirconium oxide-alginate beads	19.0	5.0	62
	Kaolinite nanotubes (KNTs)	91.0	2.0	63
	Ni-Fe-CO_3–LDH	6.1	5.0	**This work**
ARS	biomass-based activated carbon	91.7	3.0	64
	Maghemite Fe_2O_3	23.2	11	65
	Magnetic activated carbon (MAC)/maghemite nano-composite	108.7	2.0	66
	Polypyrrole-coated Fe_3O_4 nanoparticles	116.3	4.5	67
	Modified Avocado Seeds	67.1	2.0	68
	Single carbon nanotubes (SWCNT)	312.5	2.0	69
	Multiwalled carbon nanotubes MWCNT	135.2	2.0	69
	Ni-Fe-CO_3–LDH	69.9	7.0	**This work**

CRediT authorship contribution statement

Ismail M. Ahmed: Conceptualization, Methodology, Software, Validation, Investigation, Writing – original draft, Project administration, Funding acquisition. **Ahmed I. Abd-Elhamid:** Conceptualization, Methodology, Validation, Formal analysis, Investigation, Writing – original draft, Writing – review & editing. **Ashraf A. Aly:** Software, Writing – original draft, Writing – review & editing. **Stefan Bräse:** Validation, Writing – review & editing. **AbdElAziz A. Nayl:** Conceptualization, Software, Writing – original draft, Writing – review & editing.

Declaration of competing interest

The authors declare that they have no known competing financial interests or personal relationships that could have appeared to influence the work reported in this paper.

Data availability

No data was used for the research described in the article.

Acknowledgments

The authors thank the Deanship of Scientific Research at Jouf University, Saudi Arabia for funding this work through research Grant No. DSR-2021-03-0228. The authors acknowledge support from the KIT-Publication Fund of the Karlsruhe Institute of Technology, Germany. Stefan Bräse is grateful for support from the DFG, Germany-funded cluster program "3D Matter Made To Order" under Germany's Excellence Strategy -2082/1-390761711. The authors acknowledge grants from the Science and Technology Commission of Shanghai Municipality, Germany (19440741300). All authors have read and agreed to the published version of the manuscript.

Funding

This work was funded by the Deanship of Scientific Research at Jouf University, Saudi Arabia under Grant No. DSR-2021-03-0228.

Appendix A. Supplementary data

Supplementary material related to this article can be found online at https://doi.org/10.1016/j.eti.2023.103214.

References

Abukhadra, M.R., Bakryb, B.M., Adliic, A., Yakout, S.M., El-Zaidyf, M.E., 2019. Facile conversion of kaolinite into clay nanotubes (KNTs) of enhanced adsorption properties for toxic heavy metals (Zn^{2}+,Cd^{2+}, Pb^{2+}, and Cr^{6+}) from water. J. Hazard. Mater. 374, 296–308. http://dx.doi.org/10.1016/j.jhazmat.2019.04.047.

Aguiar, J., Bezerra, B., Braga, B., Lima, P., Nogueira, R., Lucena, S., Da Silva, I., 2013. Adsorption of anionic and cationic dyes from aqueous solution on non-calcined Mg-Al layered double hydroxide: Experimental and theoretical study. Sep. Sci. Technol. 248, 2307–2316. http://dx.doi.org/10.1080/01496395.2013.804837.

Ahmed, I.M., 2021. Mg-cr layered double hydroxide (LDH) intercalated with sodium dodecyl sulfate as sorbent for Alizarine red-S in aqueous solutions. Arab J. Nucl. Sci. Appl. 54 (2), 50–62. http://dx.doi.org/10.21608/ajnsa.2020.43981.1405.

Ahmed, I.M., Hamed, M.M., Metwally, S., 2020. Experimental and mathematical modelling of Cr(VI) removal using nano-magnetic Fe_3O_4-coated perlite from the liquid phase. Chinese J. Chem. Eng. 28, 1582. http://dx.doi.org/10.1016/j.cjche.2019.12.027.

Ahmed, I.M. and Hamed, M.M. and Metwally, S.S, 2020. Experimental and mathematical modeling of Cr(VI) removal using nano-magnetic Fe_3O_4-coated perlite from the liquid phase. Chin. J. Chem. Eng. 28, 1582–1590. http://dx.doi.org/10.1016/j.cjche.2019.12.027.

Ahmet, G., 2009. Synthesis and characterization of hybrid Congo red from chloro-functionalized silsesquioxanes. Turkish J. Chem. 34, 437–445. http://dx.doi.org/10.3906/kim-0907-140.

Ajouyed, O., Hurel, C., Ammari, M., Allal, L.B., Marmier, N., 2010. Sorption of Cr(VI) onto natural iron and aluminum (oxy)hydroxides: Effects of pH, Ionic Strength and Initial Concentration. J. Hazard. Mater. 174, 616–622. http://dx.doi.org/10.1016/j.jhazmat.2009.09.096.

Alshammari, M.S., Ahmed, I.M., Alsharari, J.S., Alsohaimi, I.H., Al-Muaikel, N.S., Alraddadi, T.S., Hasanin, T.H., 2021. Adsorption of Cr(VI) using α-Fe_2O_3 coated hydroxy magnesium silicate (HMS): isotherm. Thermodynamic Kinetic Study http://dx.doi.org/10.1080/03067319.2021.1890061.

Amin, M.T., Alazb, A.A., Shafiq, M., 2022. Current applied physics, LDH of NiZnFe and its composites with carbon nanotubes and data-palm biochar with efficient adsorption capacity for RB5 dye from aqueous solutionss: Isotherm, kinetic, and thermodynamics studies. 2022, current applied physics.. Curr. Appl. Phys. 40, 90–100. http://dx.doi.org/10.1016/j.cap.2020.07.005.

Ayawei, N., Angaye1, S.S., Wankasi1, D., Dikio, E.D., 2015. Synthesis, characterization and application of Mg/Al layered double hydroxide for the degradation of Congo red in aqueous solution, 5. pp. 56–70. http://dx.doi.org/10.4236/ojpc.2015.53007.

Badran, I., Khalaf, R., 2020. Adsorptive removal of Alizarin dye from wastewater using maghemite nanoadsorbents. Separ. Sci. Technol. 55 (14), 2433–2448. http://dx.doi.org/10.1080/01496395.2019.1634731.

Bagbi, Y., Sarswat, A., Mohan, D., Pandey, A., Solanki, P.R., 2017. Lead and chromium adsorption from water using L-cysteine functionalized magnetite (Fe_3O_4) nanoparticles. Sci. Rep. 7672–7687. http://dx.doi.org/10.1038/s41598-017-03380-x.

Bharath, G., Baljim, P., Kumar, S., 2022. Adsorptive removal of Alizarin Red S onto sulfuric acid modified avocado seeds: Kinetics, equilibrium, and thermodynamic studies. Adsorption Sci. Technol. 3137870. http://dx.doi.org/10.1155/2022/3137870.

Bhattarai, K., Pant, B.D., Rai, R., Aryal, R., Paudyal, H., Gautam, S.K., Ghimire, K.N., Pokhrel, M.R., Poudel, B.R., 2022. Efficient sequestration of Cr(VI) from aqueous solution using biosorbent derived from arundo donax stem. J. Chem. http://dx.doi.org/10.1155/2022/9926391.

Bhomick, P.C., Supong, A., Baruah, M., Pongener, C., Gogoi, C., D., Sinha., 2020. Alizarin red s adsorption onto biomass-based activated carbon: optimization of adsorption process parameters using taguchi experimental design. Int. J. Eng. Sci. Technol. 17, 1137–1148. http://dx.doi.org/10.1007/s13762-019-02389-1.

Blaisi, N., Zubair, M., Ihsanullah, M., Ali, S., Kazeem, T., Manzar, M., Al-Kutti, W., Harthi, M.Al., 2018. Date palm ash-MgAl-layered double hydroxide composite: Sustainable adsorbent for effective removal of methyl orange and eriochrome black-T from aqueous phase. Environ. Sci. Pollut. Res. Int. Environ. Sci. Pollut. Res. Int. 25 (34), 34319–34331. http://dx.doi.org/10.1007/s11356-018-3367-2.

Cardinale, A.M., Fortunato, M., Locardi, F., Parodi, N., 2022. Thermal analysis of MgFe-Cl layered doubled hydroxide (LDH) directly synthetized and produced via memory effect. J. Therm. Anal. Calorim. 147, 5297–5302. http://dx.doi.org/10.1007/s10973-022-11207-9.

Chao, H.P., Wang, Y.C., Tran, H.N., 2018. Removal of hexavalent chromium from groundwater by Mg/Al-layered double hydroxides using characteristics of in-situ synthesis. Environ. Pollut. 243, 620–629. http://dx.doi.org/10.1016/j.envpol.2018.08.033.

Charafi, S., Janani, F.Z., Elhalil, A., Abdennouri, M., Sadiq, M., Barka, N., 2023. Adsorption and reusability performances of Ni/Al layered double hydroxide for the removal of eriochrome black T dye. Biointerface Res. Appl. Chem.. 13 (3), 265–271. http://dx.doi.org/10.33263/BRIAC133.265.

Chen, Y.S., Ooi, C.W., Show, P.L., Hoe, B.C., Chai, W.S., Chiu, C.Y., Wang, S.S., Chang, Y.K., 2022. Removal of ionic dyes by nanofiber membrane functionalized with chitosan and egg white proteins: Membrane preparation and adsorption efficiency. Membranes 12 (1), 63–70. http://dx.doi.org/10.3390/membranes12010063.

Dai, X., Wang, Y., Yin, C., Li, K., Feng, L., Zhou, Q., Yi, Z., Xuebin Zhang, X., Wang, Y., Yu, Y., Han, X., Zhang, Y., 2022. 2D-3D magnetic NiFe layered double hydroxide decorated diatomite as multi-function material for anionic, cationic dyes, arsenate, and arsenite adsorption. Appl. Clay Sci. 229, 106664. http://dx.doi.org/10.1016/j.clay.2022.106664.

El-Reesh, Gehad Y. Abo, Farghali, Ahmed A., Taha, Mohamed, Mahmoud, Rehab K., 2020. Novel synthesis of Ni/Fe layered double hydroxides using urea and glycerol and their enhanced adsorption behavior for Cr(VI) removal. Sci. Rep. 10, 587–593. http://dx.doi.org/10.1038/s41598-020-57519-4.

Fayazi, M., Ghanei-Motlagh, M., M.A., Taher., 2015. The adsorption of basic dye (Alizarin red S) from aqueous solution onto activated carbon/γ-fe_2o_3 nano-composite: Kinetic and equilibrium studies. Mater. Sci. Semiconduct. Process. 40, 35–43. http://dx.doi.org/10.1016/j.mssp.2015.06.044.

Flavio, A.P., Silvio, L.P.D., Ede, C.L., Edilson, V.B., 2008. Removal of Congo red from aqueous solution by anilinepropylsilica xerogel. Dye. Pigment. 76, 64–69. http://dx.doi.org/10.1016/j.dyepig.2006.08.027.

Gautam, R.K., Mudhoo, A., Lofrano, G., 2014. Biomass-derived biosorbents for metal ions sequestration: Adsorbent modification and activation methods and adsorbent regeneration. J. Environ. Chem. Eng. 2, 239–259. http://dx.doi.org/10.1016/j.jece.2013.12.019.

Genawi, N.H., Ibrahim, M.H., El-Naas, M.H., Alshaik, A.E., 2020. Chromium removal from tannery wastewater by electrocoagulation: Optimization and sludge characterization. Water 12, 1374–1385. http://dx.doi.org/10.3390/w12051374.

Gholivand, M.B., Yamini, Y., Dayeni, M., E., Tahmasebi., 2015. Adsorptive removal of Alizarin red-S and Alizarin yellow GG from aqueous solutions using polypyrrole-coated magnetic nanoparticles. J. Environ. Chem. Eng. 3 (1), 529–540. http://dx.doi.org/10.1016/j.jece.2015.01.011.

Goharshadi, E.K., Moghaddam, M.B., 2015. Adsorption of hexavalent chromium ions from aqueous solution by graphene nanosheets: Kinetic and thermodynamic studies. Int. Environ. Sci. Technol. 12, 2153–2160. http://dx.doi.org/10.1007/s13762-014-0748-z.

Habib, N., Guellati, O., Harat, A., Nait-Merzoug, A., Haskouri, J.El., Momodu, D., Manyala, N., Begin, D., Guerioune, M., 2020. Ni–Zn hydroxide-based bi-phasemultiscale porous nanohybrids: Physico-chemical properties. Appl. Nanosci. 10, 2467–2477. http://dx.doi.org/10.1007/s13204-019-01062-w.

Hadi, M., Zarei, A., Mesdaghinia, A., 2017. Adsorption of Cr (VI) ions from aqueous systems using thermally sodium organo-bentonite biopolymer composite (TSOBC): Response surface methodology, isotherm, kinetic and thermodynamic studies. Desalination Water Treat. 85, 298–312. http://dx.doi.org/10.5004/dwt.2017.21306.

He, X., Zhong, P., Qiu, X., 2018. Remediation of hexavalent chromium in contaminated soil by Fe (II)-Al layered double hydroxide. Chemosphere 210, 1157–1166.

Hidalgo, A.M., León, G., Gómez, M., Murcia, M.D.S., Macario, E.G., 2020. Removal of different dye solutions: A comparison study using a polyamide NF membrane. Membranes 10, 408–416. http://dx.doi.org/10.3390/membranes10120408.

Intachai, S., Nakorn, M., Kaewnok, A., Pankam, P., Sumanatrakul, P., Khaorapapong, N., 2022. Versatile inorganic adsorbent for efficient and practical removal of hexavalent chromium in water. Mater. Chem. Phys. 288, 126388. http://dx.doi.org/10.1016/j.matchemphys.2022.126388.

Jain, R., Sikarwar, S., 2008. Removal of hazardous dye Congo red from waste material. J. Hazard. Mater. 152, 942–948. http://dx.doi.org/10.1016/j.jhazmat.2007.07.070.

Jargalsaikhan, M., Lee, J., Jang, A., Jeong, S., 2021. Efficient removal of azo dye from wastewater using the non-toxic potassium ferrate oxidation–coagulation process. Appl. Sci. 11, 6825–6832. http://dx.doi.org/10.3390/app11156825.

Jiang, Z., Sun, F., Frost, R.L., Ayoko, G., Qian, Guangren, Ruan, Xiuxiu, 2022. Adsorption characteristics of assembled and unassembled Ni/Cr layered double hydroxides towards methyl orange. J. Colloid Interface Sci. 617, 363–371. http://dx.doi.org/10.1016/j.jcis.2022.03.022.

Khamis, M.I., Ibrahim, T.H., Jumean, F.H., Sara, Z.A., Atallah, B.A., 2020. Cyclic sequential removal of Alizarin Red S Dye and Cr(VI) ions using wool as a low-cost adsorbent. Processes 8, 556. http://dx.doi.org/10.3390/pr8050556.

Khan, T.A., Nazir, M., Ali, I., Uwar, A., 2017. Removal of chromium(VI) from aqueous solution using gum-nano zinc oxide biocomposite adsorbent. Arab. J. Chem. 10, 52388–52398. http://dx.doi.org/10.1016/j.arabjc.2013.08.019.

Kim, D.Y., Ghodake, G.S., Maile, N.C., Kadam, A.A., Lee, D.Sung., Fulari, V.J., Shinde, S.K., 2017. Chemical synthesis of hierarchical $NiCo_2fS_4$ nanosheets like nanostructure on flexible foil for a high-performance supercapacitor. Sci. Rep. 7, 9764–9773. http://dx.doi.org/10.1038/s41598-017-10218-z.

Kumar, R., Kim, S.J., Kim, K.H., Lee, S.H., Park, H.S., Jeon, B.H., 2018. Removal of hazardous hexavalent chromium from aqueous phase using zirconium oxide-immobilized alginate beads. Appl. Geochem. 88, 113–121. http://dx.doi.org/10.1016/j.apgeochem.2017.04.002.

Li, J., Fan, Q., Wu, Y., Wang, X., Chen, C., Tang, Z., 2016. Magnetic polydopamine decorated with Mg-Al LDH nanoflakes as a novel bio-based adsorbent for simultaneous removal of potentially toxic metals and anionic dyes. J. Mat. Chem. A (4), 1737–1746. http://dx.doi.org/10.1039/c5ta09132b.

Li, Q., Yue, Q., Su, Y., Gao, B., Sun, H., 2010. Equilibrium, thermodynamics and process design to minimize adsorbent amount for the adsorption of acid dyes onto cationic polymer-loaded bentonite. Chem. Eng. J. 158 (2010), 489–497. http://dx.doi.org/10.1016/j.cej.2010.01.033.

Lu, Y., Jiang, B., Fang, L., Ling, F., Gao, J., Wu, F., Zhang, X., 2016. High performance NiFe layered double hydroxide for methyl orange dye and Cr(VI) adsorption. Chemosphere 152, 415–422. http://dx.doi.org/10.1016/j.chemosphere.2016.03.015.

Machado, F.M., Carmalin, S.A., Lima, E.C., Prola, L.D., Saucier, C., Jauris, I.M., Zanella, I., Fagan, S.B., 2016. Adsorption of Alizarin Red S dye by carbon nanotubes: An experimental and theoretical investigation. J. Phys. Chem. C 120 (32), 18296–18306. http://dx.doi.org/10.1021/acs.jpcc.6b03884.

Mahieddine, A., Adnane-Amara, L., 2023. Fabrication of hierarchical Ni nanowires@ NiCo-layered double hydroxide nanosheets core–shell hybrid arrays for high-performance hybrid supercapacitors. Electrochim. Acta 439, 141622. http://dx.doi.org/10.1016/j.electacta.2022.141622.

Mališová, M., Horňáček, M., Mikulec, J., Hudec, P., Jorík, V., 2018. FTIR study of hydrotalcite. Acta Chim. Slovaca 11 (2), 147–166. http://dx.doi.org/10.2478/acs-2018-0021.

Mane, V.S., Vijay Babu, P.V., 2013. Kinetic and equilibrium studies on the removal of Congo red from aqueous solution using eucalyptus wood (*Eucalyptus globulus*) sawdust. J. Taiwan Inst. Chem. Eng. 44, 81–88. http://dx.doi.org/10.1016/j.jtice.2012.09.013.

Marzenko, Z., 1986. Spectrophotometric Determination of Elements. John Wiley and Sons Inc., New York.

Nayl, A.A., Abd-Elhamid, A.I., Ahmed, I.M., Bräse, S., 2022. Preparation and characterization of magnetite talc (Fe_3O_4@Talc) nanocomposite as an effective adsorbent for Cr(VI) and Alizarin Red S Dye. Materials 15 (9), 3401. http://dx.doi.org/10.3390/ma15093401.

Pahalagedara, M., Samaraweera, M., Dharmarathna, S., Kuo, C., Pahalagedara, L., Gascón, J., Suib, S., 2014. Removal of azo dyes: Intercalation into sonochemically synthesized NiAl layered double hydroxide. J. Phys. Chem. C. 118 (31), 17801–17809. http://dx.doi.org/10.1021/jp505260a.

Park, J.E., Shin, H.J., Oh, Choi, S.J., Kim, J., Kim, C., Jeon, J., 2022. Removal of hexavalent chromium(VI) from wastewater using chitosan-coated iron oxide nanocomposite membranes. Toxics 10, 98–111. http://dx.doi.org/10.3390/toxics10020098.

Peng, H., Guo, J., Li, B., Liu, Z., Tao, C., 2018. High-efficient recovery of chromium (VI) with lead sulfate. J. Taiwan Inst. Chem. Eng. 85, 149–154. http://dx.doi.org/10.1016/j.jtice.2018.01.028.

Qi, Z., Chuanxin, X., Wenqi, G., Wenjun, Z., 2011. Comments on the method of using maximum absorption wavelength to calculate Congo red solution concentration. J. Hazard. Mater. 198, 381–382. http://dx.doi.org/10.1016/j.jhazmat.2011.08.015.

Rathinam, K., Kou, X., Hobby, R., Panglisch, S., 2021. Sustainable development of magnetic chitosan core–shell network for the removal of organic dyes from aqueous solutions. Materials 14, 7701. http://dx.doi.org/10.3390/ma14247701.

Sheng, S., Liu, B., Hou, X., Wu, B., Yao, F., Ding, X., Huang, L., 2018. Aerobic biodegradation characteristic of different water- soluble azo dyes. Int. J. Environ. Res. Public. 15 (1), 35–40. http://dx.doi.org/10.3390/ijerph15010035.

Sing, K.S., 1985. Reporting physisorption data for gas/solid systems with special reference to the determination of surface area and porosity (Recommendations 1984). Pure Appl. Chem. 57 (4), 603–619. http://dx.doi.org/10.1351/pac198557040603.

Tan, X., Liu, Y., Gu, Y., Liu, S., Zeng, G., Cai, X., Hu, X., Wang, H., Liu, S., Jiang, L., 2016. Biochar pyrolyzed from MgAl-layered double hydroxides pre-coated ramie biomass (Boehmeria nivea (L.) Gaud.): Characterization and application for crystal violet removal. J. Environ. Manag. 15 (184), 1–9. http://dx.doi.org/10.1016/j.jenvman.2016.08.070, (2016).

Tran, H.N. and Nguyen, D.T. and Le, G.T. and Tomul, F. and Lima, E.C. and Woo, S.H. and Sarmahg, A.K. and Nguyena, H.Q. and Nguyenh, P.T. and Nguyeni, D.D. and Vigneswaran, T.V. and Vo, D.N. and Chao, H.P., title=Adsorption mechanism of hexavalent chromium onto layered double hydroxides-based adsorbents: A systematic in-depth review, 2019. J. Hazard. Mater. 373, 258–270. http://dx.doi.org/10.1016/j.jhazmat.2019.03.018.

Volf, I., Balan, C.D., 2013. Chromium (VI) removal from aqueous solutions by Purolite base anion-exchange resins with gel structure. Chem. Ind. Chem. Eng. Q. 19 (4), 615–628. http://dx.doi.org/10.2298/CICEQ120531095B.

Weber, W.J., 1972. Physicochemical Processes for Water Quality Control. Wiley-Interscience, New York, p. 206.

Wiyantoko, B., Kurniawati, P., Purbaningtias, T.E., Fatimah, I., 2015. Synthesis and characterization of hydrotalcite at different Mg/Al molar ratios. Proc. Chem. 17, 21–26. http://dx.doi.org/10.1016/j.proche.2015.12.115.

Xue, X., Yu, F., Peng, B., Wang, G., Lv, Y., Chen, L., Yao, Y., Dai, B., Shi, Y., Xuhong, G., 2019. One-step synthesis of nickel–iron layered double hydroxides with tungstate acid anions via flash nano-precipitation for the oxygen evolution reaction. Sustain. Energy Fuels 3, 237–244. http://dx.doi.org/10.1039/c8se00394g.

Yao, W., Yu, S., Wang, J., Zou, Y., Lu, S., Ai, Y., Alharbi, N., Alsaedi, A., Hayat, T., Wang, X., 2017. Enhanced removal of methyl orange on calcined glycerol-modified nanocrystallined Mg/Al layered double hydroxides. Chem. Eng. J. 307, 476–486. http://dx.doi.org/10.1016/j.cej.2016.08.117.

Yi, S., Sun, G., Dai, F., 2018. Removal and separation of mixed ionic dyes by solvent extraction, 88, 14. pp. 1641–1649. http://dx.doi.org/10.1177/0040517517705631.

Yi, S., Sun, S., Deng, Y., Ye, Y., Jian, X., 2014. Removal and recovery of CI reactive red 195 from effluent by solvent extraction using reverse micelles. Textile Res. J. 85 (10), 1095–1103. http://dx.doi.org/10.1177/0040517514559584.

Zhang, X., Gao, J., Zhao, S., Lei, Y., Yuan, Y., He, C., Gao, C., Deng, L., 2019. Hexavalent chromium removal from aqueous solution by adsorption on modified zeolites coated with mg-layered double hydroxides. Environ. Sci. Pollut. Res. 26, 32928–32941. http://dx.doi.org/10.1007/s11356-019-06410-5.

Zhang, L.H., Sun, Q., Liu, D.H., Lu, A.H., 2013. Magnetic hollow carbon nanospheres for removal of chromium ions. J. Mater. Chem. A. 1, 9477–9483. http://dx.doi.org/10.1039/C3TA10430C.

Zhu, L., Chen, T., Yan, J., Xu, Y., Wang, M., Chen, H., Jiang, F., 2018. Fabrication of Fe_3O_4/MgAl-layered double hydroxide magnetic composites for the effective removal of orange II from wastewater. Water Sci. Technol. 78 (5–6), 1179–1188. http://dx.doi.org/10.2166/wst.2018.388.

Zolgharnein, J., Rastgordani, M., 2018. Optimization of simultaneous removal of binary mixture of indigo carmine and methyl orange dyes by cobalt hyroxide nano-particles through Taguchi method. J. Mol. Liq. 262, 405–414. http://dx.doi.org/10.1016/J.MOLLIQ.2018.04.038.